Journal of Sound and Vibration 333 (2014) 3382–3393

Contents lists available at ScienceDirect

Journal of Sound and Vibration

journal homepage: www.elsevier.com/locate/jsvi

Identification of Iwan distribution density function in frictional contacts

Hamid Ahmadian*, Majid Rajaei

Center of Excellence in Experimental Solid Mechanics and Dynamics School of Mechanical Engineering, Iran University of Science and Technology Narmak, Tehran 16848, Iran

ARTICLE INFO

Article history:
Received 26 July 2013
Received in revised form
4 February 2014
Accepted 13 March 2014
Handling Editor: I. Lopez Arteaga
Available online 13 April 2014

ABSTRACT

Mechanical contacts affect structural responses, causing localized nonlinear variations in the stiffness and damping. The physical behaviors of contact interfaces are quite complicated and almost impossible to model at the micro-scale. In order to establish a meaningful understanding of the friction effects and to predict the contact behavior, a robust parametric friction model is usually employed. This paper employs an Iwan-type model to predict the nonlinear effects of a frictional contact interface. The Iwan model is characterized by its distribution density function which is commonly identified by double differentiation of the experimentally obtained joint interface restoring force. Direct measurement of restoring forces at the contact interface is impractical and estimating it using an inverse approach introduces considerable uncertainties in identification of the density function. This paper develops a more reliable procedure in identification of the Iwan model by relating the density function to the joint interface dissipated energy. The energy dissipated in a contact interface is easily obtained from measurement and it is shown that the dissipation is uniquely defined using the density function and the vibration amplitude. In an experimental case study Iwan distribution density function in a frictional contact is obtained using measured dissipations at different vibration levels.

1. Introduction

Structures are commonly assembled using bolted or riveted connections. Dynamic response analysis of these structures requires accurate knowledge of the mechanisms involved in the joints and the ability to include their effects in the associated models. Detailed modeling of these mechanisms is extremely difficult as their characteristics vary significantly both during the service life and from one joint interface to another under nominally similar assembling processes and service conditions. In recent decades researchers have focused on the lumped models that resemble the role of localized stiffness, damping and its associated hysteresis loops in the joint interfaces. Efforts to improve the joint interface models' prediction capabilities have generated widespread interest in the development of different dynamic contact models.

Frictional contact interfaces have been addressed by many researchers in the past. The outlines of these research works are reviewed by Ferri [1], Berger [2] and Ibrahim and Pettit [3]. Researchers proposed many analytical/numerical models to represent the contact dynamic behavior and generate corresponding hysteresis loops. The Iwan model [4] was developed to represent the elasto-plastic behavior of materials; however, it is commonly employed to model micro-slip in contacts as

* Corresponding author. Tel.: +98 21 77240198; fax: +98 21 77240488.
E-mail address: ahmadian@iust.ac.ir (H. Ahmadian).

http://dx.doi.org/10.1016/j.jsv.2014.03.021
0022-460X/

well. The parallel-series Iwan model type is composed of parallel springs in series with coulomb friction sliders. There are some other friction models which are widely used to describe nonlinear hysteretic systems. Among them are the Bouc–Wen model [5] which is a mathematical model to generate a wide range of smooth hysteresis loops and the Valanis model [6] known from plasticity. Bristle models [7] use a statistical concept to present microscopic details of a contact surface. There are also some attempts to model joint dynamics by elementary nonlinear entities such as cubic stiffness and displacement dependent dampers in certain structures [8,9] but their range of validity is limited.

Recent studies show that the Iwan model is a promising candidate for simulating joint dynamics. Ouyang et al. [10] used the Iwan model in representing a bolted joint contact and showed that the model is capable of regenerating experimentally observed hysteresis loops. Song et al. [11] added a linear elastic spring to the Iwan model and proposed an adjusted Iwan element. The adjusted model was then used in simulating the nonlinear dynamic behavior of bolted joints in beam-like structures.

The present research work employs a formulation of idealized elements due to the Iwan model that is capable of reproducing important joint properties. The challenge in employing the Iwan model is specification of its slip force density function. One approach is to define the function in a parametric form and identify its parameters using experimentally measured data. Song et al. [11] employed an Iwan model with a uniform density function to model a jointed beam-like structure. They identified the density function parameters from a decay envelope of the structure response to impulse excitations. Shiryayev et al. [14] repeated the same practice using a similar experimental setup but under harmonic excitation force.

Segalman [15,16] provided reports on energy dissipated versus amplitude of excitation force (in the micro-slip region), and extracted some features of Iwan density function leading to a function with four unknown parameters. Iwan [4] showed that the density function can be obtained by double differentiation of joint interface restoring forces. However, accurate identification of the density function requires measurement of restoring forces at the contact interface which is impractical.

Many identification practices in this subject are based on reproducing the joint contact hysteresis loops, i.e. the parameters of model are tuned in such a way to produce the recorded hysteresis loops [10,12]. Hysteresis loops are obtained by direct measurement of the contact interface force and displacement. These measurements need special equipment and considerations especially in the case of force measurement. A second approach in obtaining the hysteresis loops is to employ an indirect method such as force state mapping [13] that requires an accurate model of the structure under investigation.

The present paper describes a method for identification of Iwan distribution density function using energy dissipated in the joint contact. The present study develops a new method to obtain more reliable friction models using the joint interface dissipation function. It shows that the dissipation is a unique function of Iwan distribution density function and the level of vibrations in the contact interface. In Section 2, the parallel-series type Iwan model formulation is briefly introduced and various means of identifying its distribution density function are discussed. Also in this section the proposed method of identifying the Iwan model slip force density function based on the relation between the contact dissipation and its vibration amplitude is developed. To demonstrate the performance of the method an experimental test setup consisting of a clamped-frictionally supported beam is employed. The test setup, the experimental measured data, and the identification procedure are reported in Section 3. In Section 4 the identified density function is used to regenerate the time domain measured responses and to validate the identified model. Finally, some conclusions are provided in Section 5.

2. Identification of Iwan distribution density function

The Iwan model in Fig. 1 consists of an infinite number of spring-slider units, called Jenkins element [4]. Jenkins element is an ideal elasto-plastic element, composed of a single discrete spring in series with a Coulomb damper characterized using a critical slipping force. The Iwan model exhibiting hysteretic characteristics suitable to model transition behavior from stick to slip appears in a joint. When an external force is applied to the model, it is distributed between Jenkins elements and some dampers, with low critical slipping force, saturate and slip. This phenomenon, known as micro-slip, causes a softening effect in the frictional sliders, stiffness and dissipates energy. As the applied force increases, more sliders saturate, and finally there would be an "ultimate force" f_y at which all dampers would slip and the macro-slip phase begins. Critical slipping

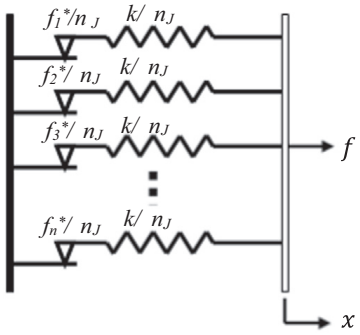

Fig. 1. The Iwan spring-slider model.

force of a frictional damper is specified by a distribution density function $\varphi(f^*)$ where $0. \le f^* \le \infty$ is the critical slipping force of its Jenkins elements.

The distribution density function can take a number of forms and when it is known, the ultimate slip force of the contact interface is determined as

$$f_y = \int_0^\infty f^* \varphi(f^*)\, \mathrm{d}f^*. \tag{1}$$

Typical hysteresis loops of an Iwan model are shown in Fig. 2. The force required to move the interface along the path from state "a" to state "b" as shown in Fig. 2 is

$$f_{a-b}(x) = \int_0^{kx} f^*\, \varphi(f^*)\, \mathrm{d}f^* + kx \int_{kx}^\infty \varphi(f^*)\, \mathrm{d}f^*, \tag{2}$$

where k is the initial contact stiffness at stick state and x is the relative movement of contacting bodies as shown in Fig. 2. The hysteresis curve is generated based on the initial load–displacement path using Eq. (2) from stick state up to the saturation state, known as "virgin curve" [16,18], in the following form:

$$f_{b-c-d}(x,A) = -\int_0^{(k(A-x)/2)} f^*\, \varphi(f^*)\, \mathrm{d}f^* + \int_{(k(A-x)/2)}^{kA} [kx - (kA - f^*)]\, \varphi(f^*)\, \mathrm{d}f^* + kx \int_{kA}^\infty \varphi(f^*)\, \mathrm{d}f^*. \tag{3}$$

In Eq. (3), A represents maximum deflection of the contact. The force required for deformation along the path "d–e–b", $f_{d-e-b}(x,A)$, is defined in a similar manner.

Iwan [4] showed that the distribution density function can be calculated from the virgin curve of the initial deformation as

$$\varphi(kx) = -\frac{1}{k^2}\frac{\partial^2 f_{a-b}}{\partial x^2}. \tag{4}$$

One may identify the distribution density function $\varphi(f^*)$ from measured force–displacement of a contact interface using Eq. (4). It is impractical to measure the restoring force of a contact interface experimentally and it is reasonable to look for alternative methods to extract the density function with less uncertainty from experimental data.

Segalman [16] proposed an alternative means of obtaining the density function from experimental data. He used the fact that energy dissipation, D, in a frictional contact is a function of the applied load, $\bar{f}$, of the following form [17]:

$$D = v\, \bar{f}^{\chi+3}, \quad -1 \le \chi \le 0, \tag{5}$$

where v is a constant. He argued the distribution density function must be of the following form to satisfy requirement (5):

$$\varphi(f^*) = R f^{*\chi}, \quad -1 \le \chi \le 0 \tag{6}$$

In Eq. (6) R is a proportionality constant. However, there are two disadvantages in employing this proposal:

2.1. Inaccuracy

The aim of the proposed distribution density function of Eq. (6) is to regenerate the power law relation between applied load and energy dissipation in the micro-slip region. The density function of Eq. (6) is capable of producing the desired values of χ with appropriate accuracy when the applied force is small. However, the proposed density function of Eq. (6) violates the requirement of Eq. (5) for large values of $\bar{f}$. A numerical simulation for the density function $\varphi(f^*) = 0.1 f^{*-0.5}$ is presented in Fig. 3. The slope of $\log(D)$ vs. $\log(\bar{f})$ in this plot, representing the power $3+\chi$, is much larger than the expected value of 2.5; the slope increases beyond the expected upper bound of 3 as applied force becomes large.

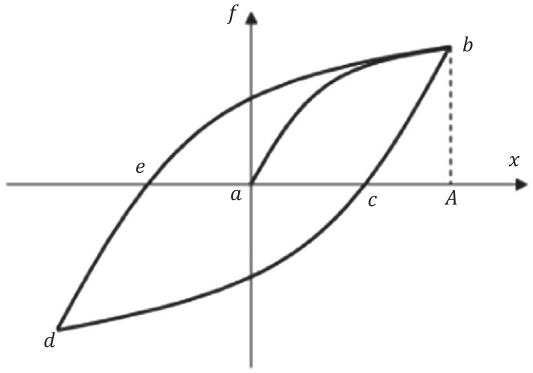

Fig. 2. A typical hysteresis loop.

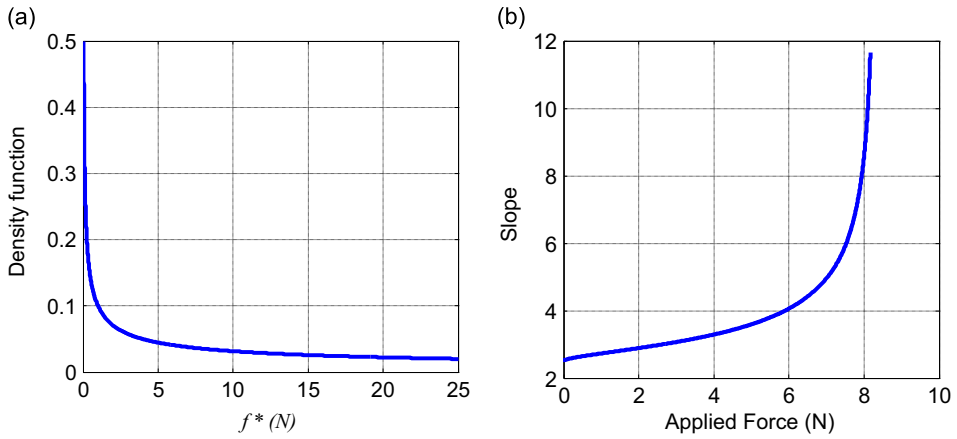

Fig. 3. The effect of density function on power law relation: (a) the density function and (b) its associated power law ($k=1$ kN/m).

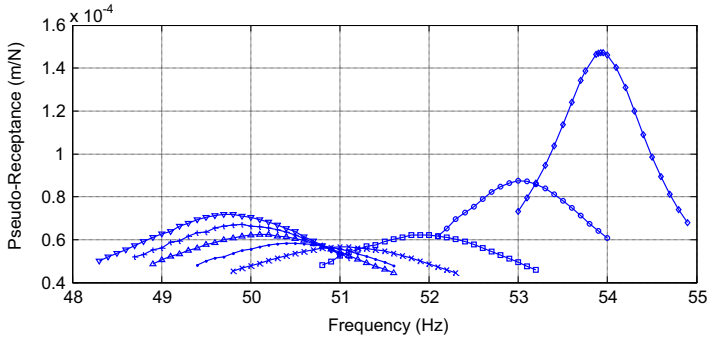

Fig. 4. Frequency responses at linear state (◇) and response amplitudes of 10^{-4} m (○), 2×10^{-4} m (□), 3×10^{-4} m (×), 4×10^{-4} m (•), 5×10^{-4} m (Δ), 6×10^{-4} m (+), and 7×10^{-4} m (∇).

2.2. Limitation

Segalman suggests that the power law relation cannot be satisfied with simple algebraic mathematical functions (i.e. constant, linear, etc.). He suggested inducing fast drop or discontinuity in the distribution density function of Eq. (6) to prevent energy dissipation from growing to large values. There are many other functions that satisfy the requirement of Eq. (5) and the proposed function in Eq. (6) is not the best candidate as it does not represent the dynamic characteristics of the contact.

This paper establishes relations between Iwan density function and contact energy dissipation; it relates the density function to the derivatives of the dissipation function w.r.t. the contact deformation. The contact interface dissipation function and its dependency on the contact deformation are extracted from experimentally measured responses.

To measure the frequency responses of nonlinear systems, two approaches are commonly employed [12]: measurement at a constant level of force excitation or at a constant level of response. The second one is usually preferred in structures with displacement dependent nonlinear phenomena such as slip. At a constant response level the nonlinear effect remains constant and its estimation by an equivalent linear system leads to a physically meaningful model. Fig. 4 shows a numerical simulation of frequency response curves for a structure with a frictional contact joint at different response amplitudes. To simulate the contact joint behavior, the Iwan model with a uniform density function is used. An increase in the response level causes the development of softening effects and the peak frequencies of FRFs decrease. The peak amplitude of FRFs, a measure of the damping ratio of the corresponding mode, initially decreases as the response amplitude level increases and then on approaching the macro-slip state, it starts to increase.

These changes in FRFs are due to micro-slip in the contact joint, and by establishing a relation between these changes and the density function one may use the FRFs as measurable data to extract the density function. However, obtaining a constant response level is time consuming and each FRF can give only two parameters (resonance frequency and damping ratio) which are not enough for accurate identification of the density function.

The damping ratio is proportional to the energy dissipation and could be measured easily [19]. As shown in Fig. 4, the damping ratio and therefore the energy dissipation, which is a good substitution for the damping ratio, have a unique changing pattern in the presence of micro-slip in the structure. This is proved by considering the dissipation over a complete loading cycle:

$$D=\oint f_{\text{joint}}(x)\,\mathrm{d}x=-2\int_{-A}^{A} f_{b-c-d}(x,A)\,\mathrm{d}x. \tag{7}$$

The derivative of energy dissipation w.r.t. joint displacement amplitude A is obtained from Eq. (7) as

$$\frac{dD}{dA} = -2\left[f_{b-c-d}(A,A)+f_{b-c-d}(-A,A)+\int_{-A}^{A}\frac{df_{b-c-d}(x,A)}{dA}\,dx\right] = 2k\int_{-A}^{A}\left[\int_{\frac{k(A-x)}{2}}^{kA}\varphi(f^*)\,df^*\right]dx. \tag{8}$$

The second derivative leads to

$$\frac{d^2D}{dA^2} = 4Ak^2\varphi(kA). \tag{9}$$

Appendix A provides the details of establishing Eqs. (8) and (9). The distribution density function is related via Eq. (9) to the energy dissipation derivatives of the contact joint in different response amplitudes. Comparing Eqs. (4) and (9), the main advantage of the proposed approach is the simplicity of measuring the energy dissipation compared to the joint restoring force. It is important to note that Eq. (9) is acceptable only when the velocity has no sign change between the upper and lower peaks of displacement. This is due to the fact that the Iwan model of Eq. (3) is unable to produce internal loops.

In the next section the proposed method is demonstrated using an experimental case study.

3. Experimental case study

3.1. The description of test setup

The test setup is the one used by the first author to identify the joint restoring forces via the force state mapping method [13]. Fig. 5 shows the test setup consisting of a slender beam clamped on one end and frictionally supported at the other end. The frictional contact boundary condition is provided using a rod attached to the beam end. A constant preload on the contact interface is provided by hanged mass blocks attached to the beam tip rod. In the mathematical model, dynamic response of the beam is considered to be governed by the Euler–Bernoulli beam theory. The geometrical and material properties of the beam are its length L, cross sectional area $\bar{A}$, cross sectional moment of inertia I, mass density ρ, modulus of elasticity E, and radius of rod r. The beam is excited by a concentrated force exerted at a distance S from the beam's clamped end. The frictional support restrains vertical movement of the beam end, but it is able to rotate or move axially.

It is worth mentioning that at higher excitation amplitudes some vertical movement occurs causing micro-slaps at the boundary. This paper considers the behavior of the system at excitation amplitudes that micro-slaps do not occur and the frictional support is in the micro/macro-slip state.

The equation governing dynamic response of the test structure shown in Fig. 5 can be expressed as

$$EI\frac{\partial^4 w}{\partial x^4}(1+i\eta) - N(t)\frac{\partial^2 w}{\partial x^2} + \rho\bar{A}\frac{\partial^2 w}{\partial t^2} = f(t)\delta(x-S) - rN(t)\delta'(x-L), \tag{10}$$

where $N(t)$ is the nonlinear friction force at the joint interface. The response of the system is obtained by expanding it using the frictionally supported beam nonlinear normal modes. The nonlinear modes are defined as the deformed shapes of the equivalent linearized system at the same response amplitude level [20]. The natural frequencies of the test structure are well separated and the structure response is expressed via n nonlinear normal modes as

$$w(x,t) = \sum_{i=1}^{n}\tilde{\phi}_i(x,a)q_i(t). \tag{11}$$

Using this series expansion and the orthogonal properties of equivalent linearized modes at response amplitude level a, the nonlinear equation of motions is transformed to the following form:

$$\ddot{q}_i(t)+i\eta_i\omega_i^2(a)q_i(t)+\omega_i^2(a)q_i(t)-f(t)\tilde{\phi}_i(S,a)-k_\theta(a)\left(\sum_{r=1}^{n}q_r(t)\frac{\partial\tilde{\phi}_r(L,a)}{\partial x}\right)\frac{\partial\tilde{\phi}_i(L,a)}{\partial x}$$
$$=\left(r\frac{\partial\tilde{\phi}_i(L,a)}{\partial x}-\sum_{r=1}^{n}q_r(t)\int_0^L\frac{\partial\tilde{\phi}_r(x,a)}{\partial x}\frac{\partial\tilde{\phi}_i(x,a)}{\partial x}\,dx\right)N(t),\ i=1,2,\ldots,n. \tag{12}$$

In Eq. (12) $k_\theta(a)$ is the support equivalent flexural stiffness at vibration levels of a. All the terms in Eq. (12), except for the friction force, are known from measurements.

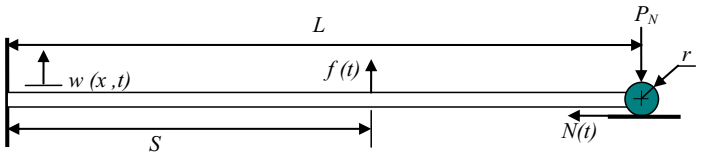

Fig. 5. A schematic view of the beam.

The relative movement of the joint interface includes three different effects expressed as

$$u(t) = -\frac{1}{2}\int_0^L \left(\frac{\partial w(x,t)}{\partial x}\right)^2 \mathrm{d}x + r\frac{\partial w(L,t)}{\partial x} + \frac{N(t)L}{\bar{A}E}. \tag{13}$$

The first term is a shortening effect of the beam due to its lateral movement. The second and third terms represent movement due to rotation of the beam end and its axial displacement, respectively.

Integration of Eq. (12) over one vibration cycle causes the first and third terms to vanish. Summation over $i=1,2,..$ and performing the same integration result in the fifth term vanishing as well:

$$\oint \left[\sum_{i=1}^{n} k_\theta(a)\frac{\partial \tilde{\phi}_i(L,a)}{\partial x}\sum_{r=1}^{n}\frac{\partial \tilde{\phi}_r(L,a)}{\partial x}q_r(t)\right]\mathrm{d}q_i(t) = \oint \mathrm{d}\left[\sum_{r=1}^{n}\frac{\partial \tilde{\phi}_r(L,a)}{\partial x}q_r(t)\right]^2 = 0. \tag{14}$$

In other words, the work of conservative forces in the system over one cycle is zero. The fourth term defines the input energy to the system as

$$\sum_{i=1}^{n}\tilde{\phi}_i(S,a)\oint f(t)\,\mathrm{d}q_i(t) = \oint f\,\mathrm{d}\left[\sum_{i=1}^{n} q_i(t)\tilde{\phi}_i(S,a)\right] = \oint f(t)\,\mathrm{d}w(S,t) = W_{\mathrm{Ext}}, \tag{15}$$

and the right-hand side of Eq. (12) defines the energy dissipated at the contact interface. If the linear damping coefficients are negligible, the input energy would be equal to the dissipated energy in the contact interface. However, in this experiment, it was observed that even in high amplitude of vibrations, the dissipation associated with linear damping is about 15 percent of the total energy dissipated. The dissipation at the contact interface is

$$-W_{\mathrm{Ext}} + \sum_{i=1}^{n}\oint i\eta_i\omega_i^2 q_i(t)\mathrm{d}q_i(t) = \sum_{i=1}^{n} r\frac{\mathrm{d}\tilde{\phi}_i(L,a)}{\mathrm{d}x}\oint N(t)\mathrm{d}q_i(t) - \sum_{i=1}^{n}\left[\sum_{j=1}^{n}\int_0^L \frac{\mathrm{d}\tilde{\phi}_i(x,a)}{\mathrm{d}x}\frac{\mathrm{d}\tilde{\phi}_j(x,a)}{\mathrm{d}x}\,\mathrm{d}x\oint N(t)q_j(t)\mathrm{d}q_i(t)\right]. \tag{16}$$

The right-hand side of Eq. (16) defines the work of the friction force which is hard to measure. However, by measuring the response at the point where force is applied, the input energy to the system is determined. When the linear damping coefficients are known, the left-hand side of Eq. (16) is known and it is equal to the energy dissipated from the contact interface.

To measure joint displacements, nonlinear normal modes are required. To obtain them, it is supposed that a torsional spring is attached to the beam end. Changing the spring stiffness alters the resonance frequencies of the beam. The stiffness is set such that the model first resonance frequency matches the corresponding measured resonance frequency.

The first and second terms in the contact interface displacement are obtained in Eq. (13) but the third one which is due to axial displacement of the beam is a function of friction force and is impossible to calculate directly from the measurement. A laser Doppler vibrometer is used in this experiment to measure axial displacement of the beam.

In the following, experiments on the beam shown in Fig. 5 are performed and data required for determining the beam nonlinear normal modes and the density function are recorded.

3.2. Base linear model identification

The beam was excited by a B&K 4200 mini-shaker attached at a distance $S=550$ mm from the clamped end and a B&K 8200 force transducer was located between the stinger and the beam to measure the input force. Lateral response of the structure was measured by three AJB 120 accelerometers and the axial movement of the beam tip was measured using an Ometron VH1000D laser Doppler vibrometer.

Initially the test structure was excited using a low random force. The amplitude was chosen in such a way to ensure that the frictional contact interface is in the stick regime. The aim was to identify the stiffness of torsional spring at the beam tip and linear damping coefficients.

The measured frequency response for two mass blocks (14 kg) is shown in Fig. 6; the linear damping coefficients for the first three modes are $\eta_1 = 0.0028$, $\eta_2 = 0.0018$, $\eta_3 = 0.0011$. Next the linear stiffness of the Iwan model is obtained which is equivalent to the torsional spring of the beam tip. This parameter is identified by matching the model first resonance frequency with the measured one in solving the characteristic equation of the linear problem.

3.3. Density function identification procedure

Single harmonic excitations were applied to the test structure at 90 different amplitudes to generate accelerations within the range of 30 mg to 4 g at direct measurement point. In each level, the frequency of excitation was set to the resonance frequency of the structure at the corresponding level (with overall error 0.1 Hz). The resonance frequency decreased from 55.8 Hz at 30 mg to 54.6 Hz at 4 g.

Most of the theory developed for nonlinear systems relies on the fact that the structure under test is excited with a pure sine wave. However, when the structure has a strong nonlinear behavior, the response signal contains higher harmonics. It is due to the fact that the actual force applied to the structure under test is the reaction force between the exciter and the

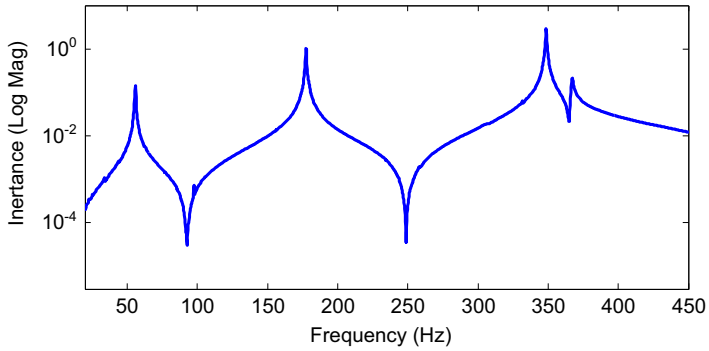

Fig. 6. Direct frequency response when contact is in the stick state.

structure. There are many algorithms to control the shaker and cancel the undesired harmonics of the force signal. Using a straightforward algorithm [21] the overall error for amplitude of undesired force harmonics is set to 1 percent of the fundamental harmonics. Fig. 7 shows measured acceleration at direct point and transmitted force to the structure.

To obtain nonlinear normal modes, the eigenvalue problem of the beam is solved. The accelerometers and force transducer mass effects are added to the model of Eq. (10). Then the beam tip end torsional spring coefficient is tuned such that the beam model generates resonance frequency equal to the one observed in the measurement. The mode shapes of the equivalent linear structure at each vibration level constitute the beam nonlinear normal modes [20].

To avoid numerical errors due to time integration, first a10th-order Fourier series is fitted to the measured acceleration data; next analytical integration is preformed to obtain the velocity and the input energy to the test structure:

$$W_{\mathrm{Ext}} = \int_0^T f(t)\,\mathrm{d}w(S,t) = \int_0^T f(t)\,\dot{w}(S,t)\,\mathrm{d}t = \Delta t \sum_{i=1}^{T/\Delta t} f_i \dot{w}(S,t_i), \tag{17}$$

where Δt is the time step. Next the modal coordinates are calculated and energy dissipated due to linear structural damping is determined:

$$W_{\text{linear damping}} = \sum_{i=1,2,3} \oint \eta_i \omega_i^2 q_i(t)\mathrm{d}q_i(t). \tag{18}$$

The contact interface dissipation is the difference between the input energy and the energy lost by linear structural damping as shown in Fig. 8 and is used in this study to identify the density function.

The Iwan distribution density function is extracted using joint displacement amplitude and its corresponding energy dissipation using Eq. (9). Fig. 9 shows the first and second derivatives of the dissipated energy, resulting in a density function identified from experimental data with no smoothing process. The obtained density function shows local oscillations in the data due to measurement errors. A global approach to differentiate experimental data using the spline smoothing method is also employed. The smoothing factors are real positive values with an upper bound of unity that corresponds to no smoothing of the experimental data. In this practice these factors are selected within the range of 0.96–0.97 to identify smooth density functions as shown in Fig. 9. The sensitivity of the generated hysteresis loops and the corresponding dissipations with different smoothing factors is investigated, and the results are shown in Fig. 10. The employed smoothing factors have little effect on the corresponding hysteresis loops, indicating successful identification of the density function.

The Iwan model of Eqs. (2) and (3) considers that the contact interface preload is constant. Therefore identification of Iwan density function is limited up to a critical slipping force f^* where there is no significant change in the contact preload. At these conditions the lap joint is not experiencing macro-slip and the area of density function remains below unity. The area under the identified density function curve is approximately 0.8 and in complete slip of interface must reach unity. No assumption about this area is made in the solution procedure, and it may be regarded as a sign of the robustness of the formulation.

At higher f^* vibro-impacts start in the presented experiment and the preload varies significantly. If one tries to reconstruct the density function in these vibration levels the identified density function would reflect the changes in the normal load and it may lose its non-negative property. Appendix B presents such a case using a numerical example.

4. Verification of the identified model

In this section, the identified density function is used to reproduce a time domain response of the structure. In regenerating the time domain response 7 mode shapes of the corresponding linear system are used.

The support nonlinearity and the beam shortening effect cause a non-symmetric displacement of the equilibrium position in the contact interface. As this happens in the steady-state response (the transient response is not symmetric in general), Eq. (3) needs to be modified to be used in evaluating the returning curve. It is assumed that the returning curve

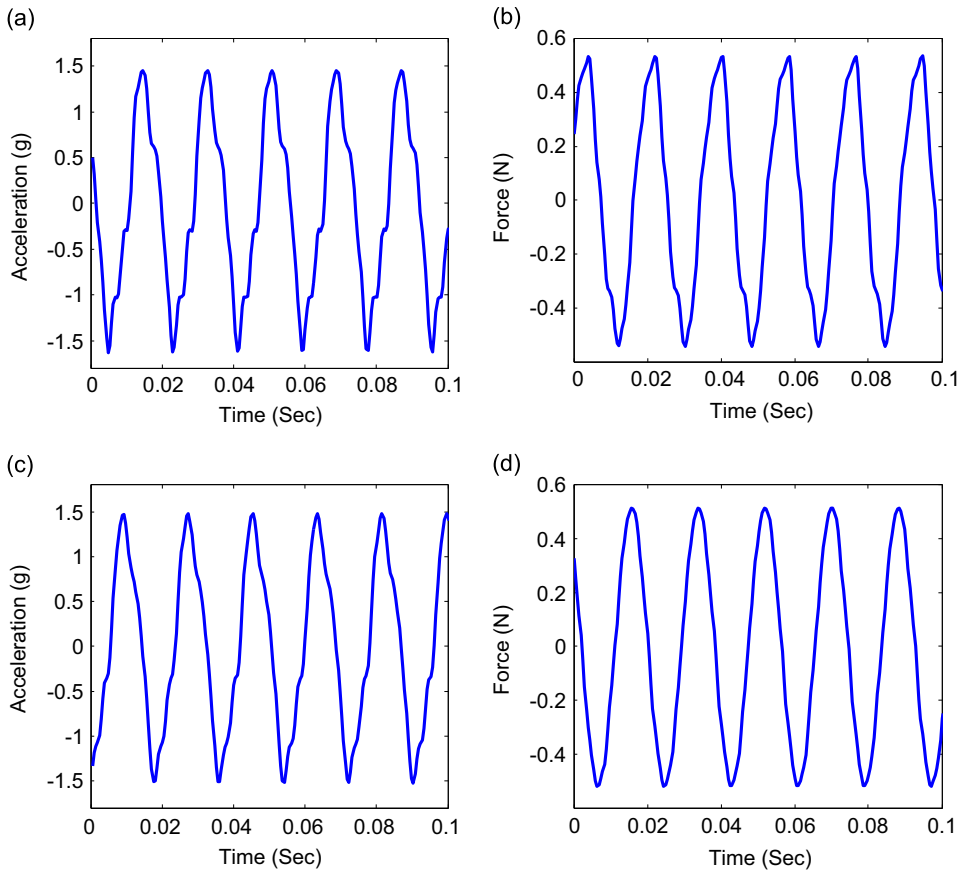

Fig. 7. Time domain data of acceleration at direct point and transmitted force: (a) and (b) before using shaker controller; (c) and (d) after using shaker controller.

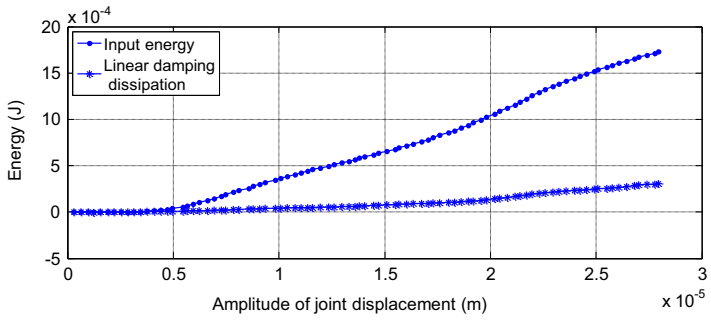

Fig. 8. The input energy and linear damping dissipation.

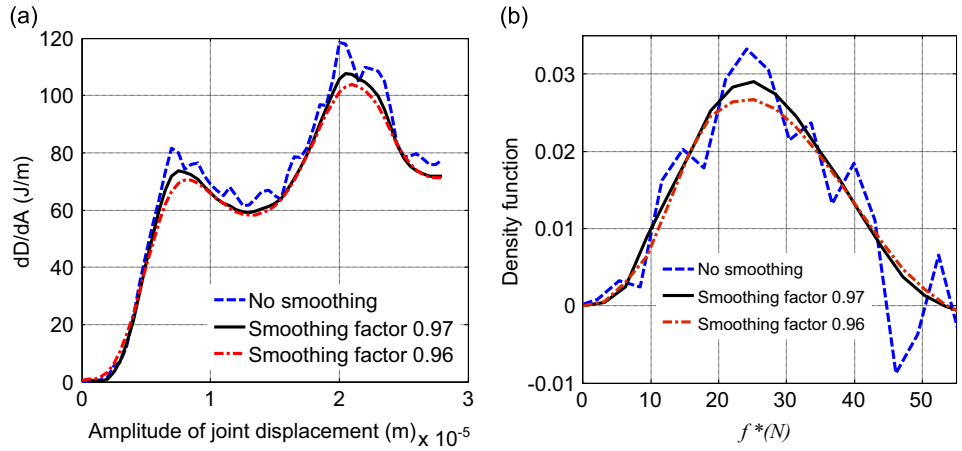

Fig. 9. (a) First derivatives of the dissipated energy and (b) the identified density functions up to $f^*=55$ N.

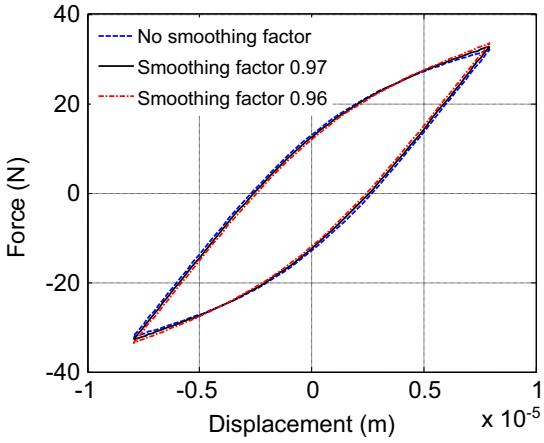

Fig. 10. The generated hysteresis loop using different smoothing factors.

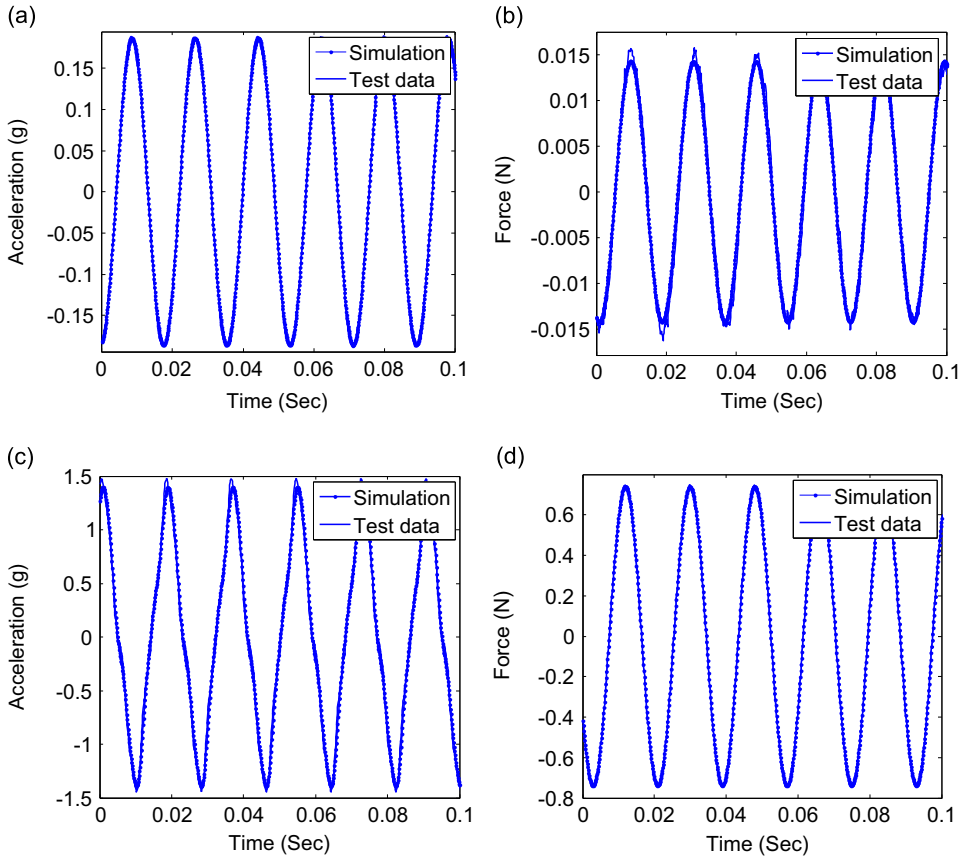

Fig. 11. Time domain of acceleration at direct point and transmitted force in two response levels: (a) and (b) at 0.2 g; (c) and (d) at 1.5 g.

f_{b-c-d} is twice the virgin curve f_{a-b} [18]; hence the joint force is determined as

$$N(u) = N(u_0) + 2N_{a-b}\left(\frac{k|(u-u_0)|}{2}\right)\mathrm{sign}(\dot{u}), \tag{19}$$

where u_0 is the point at which the contact velocity became zero.

The applied force, measured accelerations and predicted accelerations at direct point are shown in Fig. 11. There is good agreement among these results indicating successful identification of the model parameters, i.e. density function and the contact initial stiffness.

5. Conclusions

The dynamic characteristics of a beam with frictional contact support are investigated. The Iwan model is used as a natural candidate for contact modeling. It is shown that the energy dissipated in micro-slip can significantly affect the

dynamic response of the systems; hence it is used as a robust measure to identify the parameters of the Iwan contact model. The density function of the Iwan model is uniquely related to the dissipation of the contact interface and is identified with modest computational efforts. The main advantage of the proposed method is that it uses the dissipated energy in the contact interface while other methods involve the complex procedure of identifying the restoring force of the contact.

Appendix A

Dissipation in the contact joint is described as

$$D = \oint f_{\text{joint}}(x)\,\mathrm{d}x = -2\int_{-A}^{A} f_{b-c-d}(x,A)\,\mathrm{d}x. \tag{A.1}$$

The first derivative of dissipated energy w.r.t. the contact displacement amplitude is

$$\frac{\mathrm{d}D}{\mathrm{d}A} = -2\left[f_{b-c-d}(A,A)+f_{b-c-d}(-A,A)+\int_{-A}^{A}\frac{\mathrm{d}f_{b-c-d}(x,A)}{\mathrm{d}A}\mathrm{d}x\right] = -2\int_{-A}^{A}\frac{\mathrm{d}f_{b-c-d}(x,A)}{\mathrm{d}A}\mathrm{d}x. \tag{A.2}$$

The first derivative of joint force is required and by changing the integrals' limits in Eq. (3), one arrives at

$$\begin{aligned} f_{b-c-d}(x,A) &= \int_{0}^{(k(A-x)/2)} -f^*\,\varphi(f^*)\,\mathrm{d}f^* + \int_{(k(A-x)/2)}^{kA}[kx-(kA-f^*)]\varphi(f^*)\,\mathrm{d}f^* \\ &+ kx\int_{kA}^{\infty}\varphi(f^*)\,\mathrm{d}f^* = \int_{0}^{(k(A-x)/2)} -f^*\,\varphi(f^*)\,\mathrm{d}f^* + (kx-kA)\int_{(k(A-x)/2)}^{kA}\varphi(f^*)\,\mathrm{d}f^* \\ &+ \int_{(k(A-x)/2)}^{kA} f^*\varphi(f^*)\,\mathrm{d}f^* + kx\left[1-\int_{0}^{kA}\varphi(f^*)\,\mathrm{d}f^*\right]. \end{aligned} \tag{A.3}$$

The first derivative of joint restoring force is

$$\begin{aligned} \frac{\mathrm{d}f_{b-c-d}(x,A)}{\mathrm{d}A} &= \underline{\frac{k}{2}\times -1\times\frac{k(A-x)}{2}\times\varphi\left(\frac{k(A-x)}{2}\right)} \\ &+ (kx-kA)\times\left[\underline{\underline{k\times\varphi(kA)}}\underline{-\frac{k}{2}\varphi\left(\frac{k(A-x)}{2}\right)}\right] - k\int_{(k(A-x)/2)}^{kA}\varphi(f^*)\,\mathrm{d}f^* \\ &+ \underline{\underline{k\times kA\times\varphi(kA)}}\underline{-\frac{k}{2}\times\frac{k(A-x)}{2}\times\varphi\left(\frac{k(A-x)}{2}\right)}+\underline{\underline{kx\times -1\times k\times\varphi(kA)}} \\ &= -k\int_{(k(A-x)/2)}^{kA}\varphi(f^*)\,\mathrm{d}f^*. \end{aligned} \tag{A.4}$$

The terms with the same underlines cancel out each other and the first derivative of the dissipation is obtained:

$$\frac{\mathrm{d}D}{\mathrm{d}A} = 2k\int_{-A}^{A}\left[\int_{(k(A-x)/2)}^{kA}\varphi(f^*)\,\mathrm{d}f^*\right]\mathrm{d}x. \tag{A.5}$$

Rearranging the relation (A.5), one obtains

$$\begin{aligned} -\frac{1}{2}\frac{\mathrm{d}D}{\mathrm{d}A} &= -k\int_{-A}^{A}\left[\int_{(k(A-x)/2)}^{kA}\varphi(f^*)\,\mathrm{d}f^*\right]\mathrm{d}x \\ &= -k\int_{-A}^{A}\left[\int_{0}^{kA}\varphi(f^*)\,\mathrm{d}f^*\right]\mathrm{d}x + k\int_{-A}^{A}\left[\int_{0}^{(k(A-x)/2)}\varphi(f^*)\,\mathrm{d}f^*\right]\mathrm{d}x \\ &= -k\int_{0}^{kA}\left[\int_{-A}^{A}\varphi(f^*)\,\mathrm{d}x\right]\mathrm{d}f^* + k\int_{-A}^{A}\left[\int_{0}^{(k(A-x)/2)}\varphi(f^*)\,\mathrm{d}f^*\right]\mathrm{d}x \\ &= -2kA\int_{0}^{kA}\varphi(f^*)\,\mathrm{d}f + k\int_{-A}^{A}\left[\int_{0}^{(k(A-x)/2)}\varphi(f^*)\,\mathrm{d}f^*\right]\mathrm{d}x. \end{aligned} \tag{A.6}$$

And finally the second derivative of the dissipated energy is obtained:

$$\begin{aligned} -\frac{1}{2}\frac{\mathrm{d}^2D}{\mathrm{d}A^2} &= -2Ak^2\varphi(kA) - 2k\int_{0}^{kA}\varphi(f^*)\mathrm{d}f^* \\ &+ k\int_{0}^{(k(A-A)/2)}\varphi(f^*)\mathrm{d}f^* + k\int_{0}^{kA}\varphi(f^*)\mathrm{d}f^* + k\int_{-A}^{A}\frac{k}{2}\varphi\left(\frac{k(A-x)}{2}\right)\mathrm{d}x \\ &= -2Ak^2\varphi(kA). \end{aligned} \tag{A.7}$$

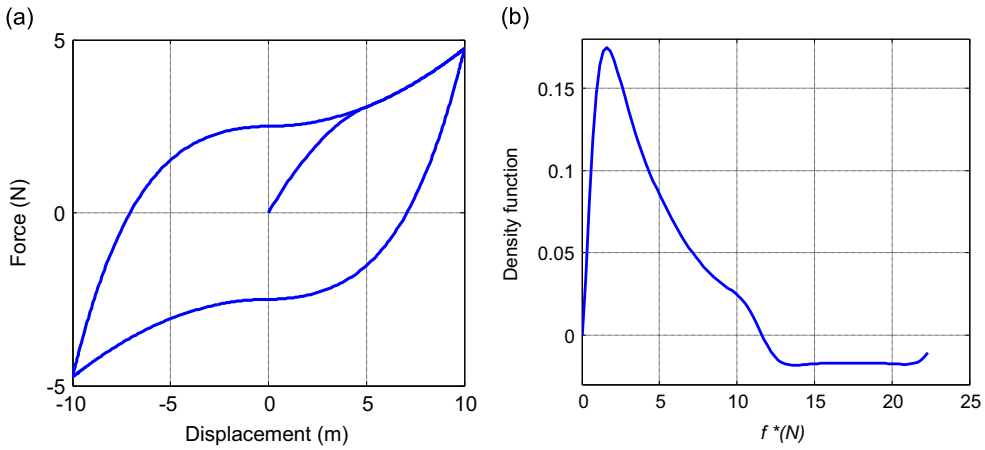

Fig. B1. The effect of variable normal load. (a) The hysteresis loop generated by Jenkins elements and (b) the density functions.

Appendix B

The effect of variable normal load is demonstrated using an Iwan model with stiffness $k=1\ N/m$ and a uniform density function which spans from 0 to 5 N as

$$\varphi(f^*)=0.2(1-\text{Heaviside}(f^*-5)), \tag{B.1}$$

The model is discretized using 200 Jenkins elements, as shown in Fig. 1, as

$$\bar{k}=\frac{k}{n_J}=\frac{1}{200}=0.005, \tag{B.2}$$

$$\bar{f}_i^*=\frac{f_i^*}{n_J}=\frac{(f_{\max}^*)(i/n_J)}{n_J}=\frac{5\times(i/200)}{200}=\frac{5}{200^2}i,\quad i=1,2,\ldots,n_J, \tag{B.3}$$

where $\bar{k}$ and $\bar{f}_i^*$ are the stiffness and slip force limit of each Jenkins element, respectively. These parameters are defined for a constant preload condition. If preload changes over one cycle, they also change and various types of hysteresis diagrams are achieved. In a simulated example the contact shear deformation $x(t)$ is assumed to be single harmonic with hypothetical normal load variations of $P_N(t)$:

$$x(t)=10\ \sin(2\pi t), \tag{B.4}$$

$$P_N(t)=P_N(1+0.9\ \sin^2(2\pi t)). \tag{B.5}$$

The effect of normal load variations on the contact stiffness and slippage force is assumed to be of a proportional form:

$$\tilde{k}=\bar{k}P_N(t),\ \ \tilde{f}_i^*=\bar{f}_i^*P_N(t). \tag{B.6}$$

where $\tilde{k}$ and $\tilde{f}_i^*$ are stiffness and slip force limit as a function of normal load, respectively. Fig. B1a shows the resultant hysteresis diagram under a variable normal load and the corresponding Iwan density function, obtained by double differentiation of the hysteresis loop.

The hysteresis loop shown in Fig. B1a has a hardening effect that is the result of increasing the preload in the middle of the returning curves. An increase in the preload has two effects:

1. The stiffness of unsaturated Jenkins elements increases.
2. The required force to slip each Jenkins element increases and results in some saturated Jenkins elements returning to the elastic deformation state.

Now if one extracts the density function using double derivative of the hysteresis loop and neglects the preload effect, the density function would have a negative value to simulate this hardening effect, as shown in Fig. B1b.

References

[1] A.A. Ferri, Friction damping and isolation systems, *Journal of Mechanical Design* 117 (1995) 196–206.
[2] E.J. Berger, Friction modeling for dynamic system simulation, *Applied Mechanics Reviews* 55 (6) (2002) 535–577.
[3] R.A. Ibrahim, C.L. Pettit, Uncertainties and dynamic problems of bolted joints and other fasteners, *Journal of Sound and Vibration* 279 (3–5) (2005) 857–936.
[4] W.D. Iwan, A distributed-element model for hysteresis and its steady-state dynamic response, *ASME Journal of Applied Mechanics* 33 (1966) 893–900.
[5] F. Ikhouane, J. Rodellar, On the hysteretic Bouc–Wen model, *Nonlinear Dynamics* 42 (2005) 63–78.

[6] K.C. Valanis, A theory of viscoplasticity without a yield surface, *Archives of Mechanics* 23 (4) (1971) 171–191.
[7] D.A. Haessig, B. Friedland, On the modeling and simulation of friction, *ASME Journal of Dynamic Systems, Measurement, and Control* 113 (1991) 354–362.
[8] H. Ahmadian, H. Jalali, Identification of bolted lap joints parameters in assembled structures, *Mechanical Systems and Signal Processing* 21 (2) (2007) 1041–1050.
[9] H. Ahmadian, H. Jalali, Generic element formulation for modeling bolted lap joints, *Mechanical Systems and Signal Processing* 21 (5) (2007) 2318–2334.
[10] H. Ouyang, M.J. Oldfield, J.E. Mottershead, Experimental and theoretical studies of a bolted joint excited by a torsional dynamic load, *International Journal of Mechanical Sciences* 48 (12) (2006) 1447–1455.
[11] Y. Song, C.J. Hartwigsen, D.M. McFarland, A.F. Vakakis, A.F. Bergman, Simulation of dynamics of beam structures with bolted joints using adjusted Iwan beam elements, *Journal of Sound and Vibration* 273 (1–2) (2004) 249–276.
[12] K.Y. Sanliturk, D.J. Ewins, Modelling two-dimensional friction contact and its application using harmonic balance method, *Journal of Sound and Vibration* 193 (1996) 511–523.
[13] H. Ahmadian, H. Jalali, F. Pourahmadian, Nonlinear model identification of a frictional contact support, *Mechanical Systems and Signal Processing* 24 (8) (2010) 2844–2854.
[14] O.V. Shiryayaev, S.M. Page, C.L. Pettit, J.C. Slater, Parameter estimation and investigation of a bolted joint model, *Journal of Sound and Vibration* 307 (2007) 680–697.
[15] D.J. Segalman, A four parameter Iwan model for lap-type joints, *Journal of Applied Mechanics Transactions of the ASME* 72 (2005) 752–760.
[16] D.J. Segalman, An Initial Overview of Iwan Modeling for Mechanical Joints, Sandia National Labs Report 2001-0811, 2001.
[17] D.O. Smallwood, D.L. Gregory, R.G. Coleman, Damping investigations of a simplified frictional shear joint, *Proceedings of the 71st Shock and Vibration Symposium*, 2000.
[18] D.J. Segalman, M.J. Starr, Inversion of Masing models via continuous Iwan systems, *International Journal of Non Linear Mechanics* 43 (2008) 74–80.
[19] D.J. Ewins, *Modal Testing: Theory, Practice and Application*, Research Studies Press Ltd, Philadelphia, 2000.
[20] W. Szemplinska-Stupnicka, The modified single mode method in the investigations of the resonant vibrations of nonlinear systems, *Journal of Sound and Vibration* 65 (1979) 475–489.
[21] A. Josefsson, M. Magnevall, K. Ahlin, Control algorithm for sine excitation on nonlinear systems, *Proceedings of the International Modal Analysis Conference IMAC-XXIV*, St. Louis, Missouri, USA, 2006.